SYMPLECTIC INTEGRATOR FOR INSERTION DEVICES TRACKING AT SIRIUS

G. R. Ascenção[1*], V. Souza[1], F. H. de Sá, X. R. Resende
Brazilian Synchrotron Light Laboratory (LNLS), Campinas, Brazil
[1]also at Gleb Wataghin Institute of Physics, University of Campinas, Campinas, Brazil

Abstract

This paper describes the development of an explicit symplectic integrator for insertion devices based on the method of Wu, Forest, and Robin, and applies it to the CPMU13, a new SIRIUS insertion device designed for operation in a high-beta straight section with a minimum gap of 4.65 mm. We detail the magnetic field fitting procedure and benchmark particle tracking results against a conventional kickmap approach.

INTRODUCTION

The Brazilian Center for Research in Energy and Materials (CNPEM) is currently developing the ORION project [1], a biosafety level 4 laboratory integrated with three beamlines of the SIRIUS synchrotron light source. One of these beamlines, HIBISCO [2], will be installed in a high-beta straight section ($\beta_x = 17.2\,\mathrm{m}$ and $\beta_y = 3.6\,\mathrm{m}$) and will employ a cryogenic permanent magnet undulator (CPMU) [3] as its photon source.

To meet the beamline requirements, the insertion device (ID) is designed with a period length of 13.6 mm and a total of 147 periods, reaching a peak magnetic field of 1.08 T at a minimum gap of 4.65 mm.

A key concern is the impact of the ID on nonlinear beam dynamics, particularly for particles with large transverse amplitudes, as encountered during injection. This is especially relevant for SIRIUS, where injection is performed off-axis using a nonlinear kicker [4]. Accurate modeling of the ID effects is therefore essential to ensure the robustness of the injection process.

Most tracking codes currently model ID effects using kickmaps [5], a well-established tool in the synchrotron community. However, kickmaps in general are not symplectic, and the impact of this non-symplecticity on long-term particle stability remains insufficiently explored in the literature. In this work, the WFR (Wu–Forest–Robin) [6] integrator is employed as a benchmark against kickmap-based tracking, enabling a more rigorous assessment of the dynamics and ensuring accurate modeling of the new CPMU at SIRIUS.

WFR INTEGRATOR FOR S-DEPENDENT MAGNETIC FIELDS

Under the paraxial approximation, the Hamiltonian describing the motion of a charged particle with charge q in Cartesian coordinates can be written in extended phase space, including (z, p_z), as

$$H(x,p_x,y,p_y,\delta,l;\sigma) = \frac{(p_x-a_x)^2}{2(1+\delta)} + \frac{(p_y-a_y)^2}{2(1+\delta)} + p_z - a_z, \tag{1}$$

where $p_i = P_i/P_0$ denotes the transverse momenta normalized to the reference momentum P_0, δ is the relative momentum deviation, l is the path length, and $a_i = qA_i/(P_0 c)$ is the normalized vector potential. The independent variable is denoted by σ.

The exact Lie map associated with a step $\Delta\sigma$ is given by

$$\mathscr{M}(\Delta\sigma) = \exp\left(-\Delta\sigma : H :\right). \tag{2}$$

In practice, a symplectic integrator is obtained by factorizing this map. Assuming the gauge $a_z = 0$, a second-order approximation of $\mathscr{M}$ can be constructed as

$$\begin{aligned}\mathscr{M}_2(\Delta\sigma) = {} & \exp\left(: -\frac{(p_z-\delta)\Delta\sigma}{2} :\right) \\ & \times \mathscr{A}_y \exp\left(: -\frac{p_y^2\Delta\sigma}{4(1+\delta)} :\right) \mathscr{A}_y^{-1} \\ & \times \mathscr{A}_x \exp\left(: -\frac{p_x^2\Delta\sigma}{2(1+\delta)} :\right) \mathscr{A}_x^{-1} \\ & \times \mathscr{A}_y \exp\left(: -\frac{p_y^2\Delta\sigma}{4(1+\delta)} :\right) \mathscr{A}_y^{-1} \\ & \times \exp\left(: -\frac{(p_z-\delta)\Delta\sigma}{2} :\right),\end{aligned} \tag{3}$$

where the operators $\mathscr{A}_i$ are defined as

$$\mathscr{A}_i = \exp\left(- : \int a_i(x,y,z)\,\mathrm{d}i :\right). \tag{4}$$

The dependence of the vector potential on the longitudinal coordinate z is naturally incorporated through the operators $\mathscr{A}_i$ [6].

GENERAL UNDULATOR MODEL FOR THE WFR INTEGRATOR

To evaluate the operators $\mathscr{A}_i$, an analytical representation of the vector potential components A_i is required. For this purpose, we adopt a Fourier-based model of the 3D static magnetic field of a planar undulator, given by

$$\begin{aligned}B_y &= \sum_{m,n} \cos(mk_x x)\cosh(k_{ymn} y)\,\left(C_{mn} f_n(z) + D_{mn} g_n(z)\right) \\ B_x &= \sum_{m,n} \frac{mk_x}{k_{ymn}} \sin(mk_x x)\sinh(k_{ymn} y)\,\left(C_{mn} f_n(z) + D_{mn} g_n(z)\right) \\ B_z &= \sum_{m,n} \frac{nk_z}{k_{ymn}} \cos(mk_x x)\sinh(k_{ymn} y)\,\left(C_{mn} g_n(z) + D_{mn} f_n(z)\right).\end{aligned} \tag{5}$$

* gabriel.ascencao@lnls.br

The longitudinal dependence is described by the functions

$$f_n(z) = \sin(nk_z z), \quad g_n(z) = \cos(nk_z z), \tag{6}$$

while the wave numbers satisfy

$$k_{ymn}^2 = m^2 k_x^2 + n^2 k_z^2. \tag{7}$$

This representation is sufficiently general to capture edge effects arising from the terminations of a planar insertion device and satisfies Maxwell equations. However, when the fit is restricted to the undulator core, either C_{mn} or D_{mn} can be set to zero depending on the symmetry of the magnetic field. For the CPMU13, the symmetry implies $D_{mn} = 0$.

In the core region, five modes were retained in each direction ($n_{\max} = 5$, $m_{\max} = 5$). For the terminations, a higher longitudinal resolution was required, with fifteen modes in the longitudinal direction and three modes in the horizontal direction ($n_{\max} = 15$, $m_{\max} = 3$). Figure 1 shows the fitting results for the CPMU magnetic field. Regions A and B correspond to the terminations, while region C denotes the undulator core.

The tracking step size is adapted to each region according to the local field characteristics. In region A, the step size is chosen to match the wavelength of the dominant fitted mode, suppressing spurious oscillations introduced by the fitting procedure, resulting in $\Delta\sigma_A = 6.6\,\text{mm}$. In region B (transition region), a finer step size is adopted, $\Delta\sigma_B = 1.11\,\text{mm}$, to better resolve the rapid field variation. In region C, the step size is selected to ensure an integer number of integration steps per undulator period, corresponding to eight points per period.

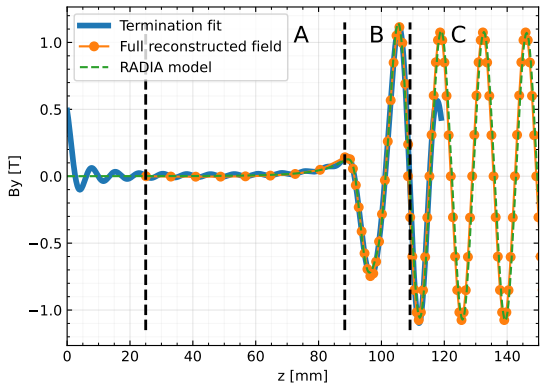

Figure 1: Vertical magnetic field $B_y(z)$. The RADIA simulation (green dashed) is compared with the Fourier-based termination fit (blue) and the reconstructed field (orange). Dashed vertical lines separate the termination (A), transition (B), and periodic regions (C).

RESULTS

Phase-Space

The WFR integrator was implemented in the `trackcpp` code [7]. A comparison of particle tracking over 15 000 turns is presented in Fig. 2. The upper panels show the horizontal phase space, with particles initialized at $x_0 = -6\,\text{mm}$, while the lower panels correspond to the vertical phase space, with $y_0 = 2\,\text{mm}$.

The left column shows results for the nominal CPMU13 magnetic field at its minimum gap (1.08 T). In this case, both the WFR integrator and the kickmap approach yield consistent results, with no significant differences observed.

The right column illustrates a scenario where the two approaches diverge. Here, the CPMU field is artificially rescaled by a factor of 6. Under these conditions, the electron is lost when using the kickmap model, whereas they remain stable with the WFR integrator, highlighting the importance of a symplectic treatment in regimes with strong nonlinearities.

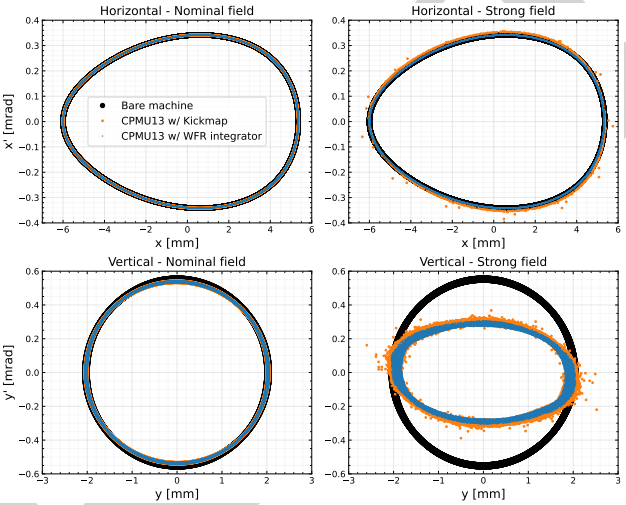

Figure 2: Phase-space trajectories over 15 000 turns for horizontal (top) and vertical (bottom) motion.

Linear Optics

The differences between the two integration methods were also evaluated in terms of linear optics. The impact of each approach on the storage ring beta functions, considering the CPMU13 at its nominal minimum field, is shown in Fig. 3. Both methods yield consistent results for the vertical plane (right panel), with similar beta beating and comparable tune shifts ($\Delta\nu_y = 3.28 \times 10^{-3}$ for the WFR integrator and $\Delta\nu_y = 3.23 \times 10^{-3}$ for the kickmap).

In contrast, significant discrepancies are observed in the horizontal plane. The kickmap approach overestimates the focusing effect of the insertion device, leading to a horizontal beta beating approximately one order of magnitude larger than that predicted by the WFR integrator, as shown in the left panel of Fig. 3. This difference is also reflected in the horizontal tune shifts, with $\Delta\nu_x = 7.16 \times 10^{-6}$ for the WFR integrator and $\Delta\nu_x = -1.28 \times 10^{-4}$ for the kickmap.

Frequency Maps and Diffusion

The impact of the non-symplectic nature of kickmaps was further investigated using frequency map analysis [8] and diffusion analysis. Figure 4 shows the diffusion obtained

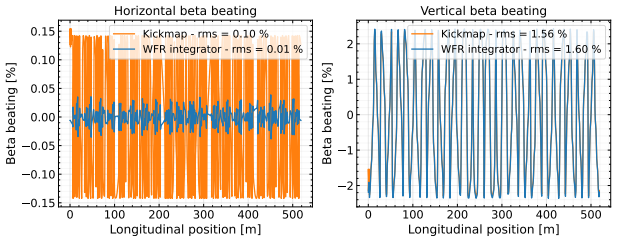

Figure 3: Horizontal (left) and vertical (right) beta beating induced by ID.

with the kickmap approach (left panel) and with the WFR integrator (right panel). The kickmap introduces significantly higher diffusion across the phase space, whereas the WFR integrator yields more stable behavior throughout the transverse (x, y) plane. Despite these differences, the dynamic aperture remains essentially unchanged in both cases.

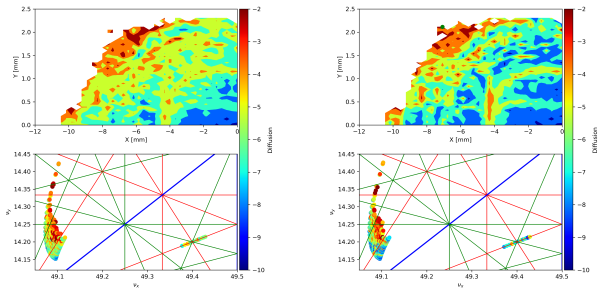

Figure 4: Frequency map analysis and diffusion in the transverse (x, y) phase space.

Dynamic Aperture

The final analysis focuses on the dynamic aperture in transverse phase space (x, y) and in the (δ, x) plane. For this study, particles were tracked for 2000 turns over an ensemble of 20 storage ring models. With each model including random errors, such as magnet and girder misalignments, excitation errors, and multipole components. The resulting dynamic apertures in the transverse plane and in energy deviation versus horizontal position are shown in Figs. 5 and 6, respectively.

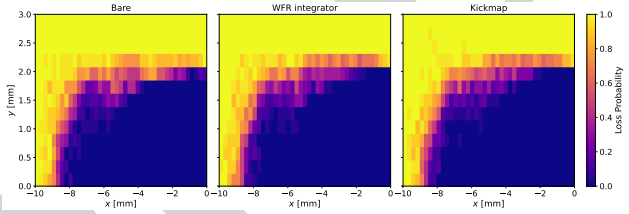

Figure 5: Dynamic aperture in the transverse (x, y) phase space for the bare machine, WFR integrator, and kickmap.

Both the kickmap and WFR integrator approaches show good agreement in terms of survival rate for the case studied. It is important to note that this agreement holds for the nominal CPMU13 field.

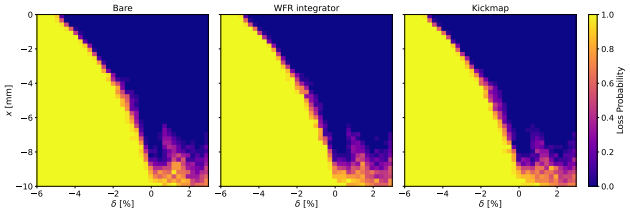

Figure 6: Dynamic aperture in the (δ, x) phase space for the bare machine, WFR integrator, and kickmap.

CONCLUSION

In this work, a WFR integrator was implemented in the *trackcpp* code and benchmarked against the kickmap approach. The comparison was performed in terms of long term tracking symplecticity, linear optics, frequency map analysis, and dynamic aperture.

Under nominal operating conditions of the CPMU13, both methods show good agreement in phase-space trajectories, survival rates, and dynamic aperture. However, the kickmap approach overestimates the horizontal focusing effect of the insertion device, leading to significantly larger horizontal beta beating and noticeable discrepancies in the horizontal tune shift.

These limitations become more evident in the frequency map analysis, where the kickmap introduces enhanced diffusion, indicating the presence of artificially increased chaos in phase space. In contrast, the WFR integrator preserves a more regular and stable dynamical structure.

For increased magnetic field strength, the discrepancies are further amplified. In this regime, the kickmap approach can lead to artificial particle loss, whereas the WFR integrator maintains stable trajectories, demonstrating its robustness in the presence of strong nonlinearities.

Overall, while kickmaps provide a computationally efficient approximation under standard conditions (approximately 30× faster), the WFR integrator offers a more accurate and reliable description of beam dynamics, particularly in regimes where nonlinear effects and long-term stability are critical.

ACKNOWLEDGEMENTS

The authors would like to thank Mostafa Muradi from the MAX IV insertion devices team for his assistance with the implementation of the Ellaume formalism used to generate the kickmap tables.

REFERENCES

[1] Brazilian Center for Research in Energy and Materials (CNPEM), 'Orion Project,' `https://cnpem.br/en/orion/`, accessed: May 2026.

[2] LNLS, "SIRIUS Beamlines", available at `https://lnls.cnpem.br/beamlines/`

[3] T. Hara *et al.*, 'Cryogenic permanent magnet undulators,' Phys. Rev. Accel. Beams, vol. 7, p. 050702, 2004. doi:10.1103/PhysRevSTAB.7.050702

[4] L. Liu, X. R. Resende, A. R. D. Rodrigues, and F. H. de Sá, "Injection Dynamics for Sirius Using a Nonlinear Kicker", in *Proc. IPAC'16*, Busan, Korea, May 2016, pp. 3406–3408. doi:10.18429/JACoW-IPAC2016-THPMR011

[5] P. Elleaume, "A New Approach to the Electron Beam Dynamics in Undulators and Wigglers", in *Proc. EPAC'92*, Berlin, Germany, Mar. 1992, pp. 661–664.

[6] Y. K. Wu, E. Forest, and D. S. Robin, 'Explicit symplectic integrator for *s*-dependent static magnetic field,' Phys. Rev. E, vol. 68, p. 046502, 2003. doi:10.1103/PhysRevE.68.046502

[7] LNLS Accelerator Physics Group, 'trackcpp: tracking code for particle accelerators,' GitHub repository, `https://github.com/lnls-fac/trackcpp`, accessed: May 2026.

[8] J. Laskar, "The chaotic motion of the solar system: a numerical estimate of the size of the chaotic zones," *Icarus*, vol. 88, no. 2, pp. 266–291, 1990. doi:10.1016/0019-1035(90)90084-M